Advances in Computational Design, *Vol. 3, No. 2 (2018) 165-190*
DOI: https://doi.org/10.12989/acd.2018.3.2.165

Static analysis of functionally graded non-prismatic sandwich beams

M. Rezaiee-Pajand*, Amir R. Masoodi and M. Mokhtari

Department of Civil Engineering, Ferdowsi University of Mashhad, Iran

(Received November 2, 2017, Revised February 12, 2018, Accepted February 14, 2018)

Abstract. In this article, the static behavior of non-prismatic sandwich beams composed of functionally graded (FG) materials is investigated for the first time. Two types of beams in which the variation of elastic modulus follows a power-law form are studied. The principle of minimum total potential energy is applied along with the Ritz method to derive and solve the governing equations. Considering conventional boundary conditions, Chebyshev polynomials of the first kind are used as auxiliary shape functions. The formulation is developed within the framework of well-known Timoshenko and Reddy beam theories (TBT, RBT). Since the beams are simultaneously tapered and functionally graded, bending and shear stress pushover curves are presented to get a profound insight into the variation of stresses along the beam. The proposed formulations and solution scheme are verified through benchmark problems. In this context, excellent agreement is observed. Numerical results are included considering beams with various cross sectional types to inspect the effects of taper ratio and gradient index on deflections and stresses. It is observed that the boundary conditions, taper ratio, gradient index value and core to the thickness ratio significantly influence the stress and deflection responses.

Keywords: static analysis; Ritz method; tapered sandwich beam; functionally graded material; Chebyshev polynomials

1. Introduction

As the manufacturing technologies have advanced during the last few decades, application of sandwich structures has been widely come into vogue in many industrial scopes. Sandwich structures consist of a thick and routinely soft core enclosed between two thin and stiff facings. Different types of such structures have been developed including FRP sandwich beams, CFRP sandwich beams, aluminum composite beams and etc. On the other hand; the main reason behind application of tapered beams is that an optimum design can be achieved using lower amounts of material. Weight savings and high flexural stiffness offered by tapered sandwich beams result in their potential application in many engineering fields such as shuttle structural elements, aerospace engineering, ships and marine structures and railroad constructions. Therefore, it of significant

*Corresponding author, Professor, E-mail: rezaiee@um.ac.ir
[a] Ph.D. Candidate, E-mail: amirreza.masoodi@mail.um.ac.ir
[b] M.Sc. Student, E-mail: ce.mahdimokhtari@gmail.com

http://www.techno-press.org/?journal=acd&subpage=7 ISSN: 2283-8477 (Print), 2466-0523 (Online)

importance to propose simple and accurate analysis methods to study the behavior of tapered sandwich structures undergoing different loading types. Energy methods based on the first-order shear deformation theory (FSDT) and finite element methods (FEM) are the well-known solutions, which have been employed for analysis of sandwich beams (Ha 1990, Vinson 1999, Hu *et al.* 2008). Nowadays, soft cores are used in advanced sandwich structures. Softness and compressibility of the core throughout the thickness affect the behavior of structure. In 1992, a new method based on the higher-order solution of the sandwich structures was proposed by Frostig et al. (Frostig *et al*. 1992). In this research, the sandwich structure was divided into three substructures, including upper and lower faces and a soft core. To model the upper and lower faces, the classical theory of plates subjected to the pure bending was employed. On the other hand, the core of the beam was modeled based on the 3D elastic theory. These three substructures were analyzed simultaneously. Moreover, the compatibility conditions of faces and core displacements at the contact position were employed to solve the governing equations analytically.

The higher-order shear deformation theories, widely known as HSDT, offer advantageous properties including consideration of various boundary conditions on the upper and lower faces. Further, compaction and shear deformation effects of the core can be modeled using these theories. It should be added that other researchers employed higher-order shear deformation theories to investigate the behavior of sandwich structures with various cross-section types subjected to different loadings. In addition, different types of boundary conditions were considered in these researches. A number of these studies are available in full detain in (Frostig and Thomsen 2004, Frostig 2009, Santiuste *et al.* 2011, Phan *et al.* 2013).

It has been proven that one of the effective parameters on the behavior of beams is their shear deformations. Various general theories are capable of incorporating the shear deformation effects into the governing equations. A number of these theories are available in the literature, including the first-order shear deformation theory (FSDT), higher-order shear deformation theory (HSDT), Carrera Unified Formulation (CUF) and quasi-3D displacement fields. In the FSDT, the shear strain varies linearly along the height of the cross section. To satisfy the stress-free boundary conditions at the upper and lower surfaces, a shear correction factor should be utilized (Nguyen, Vo *et al.* 2014, Thai *et al*. 2014). In contrast, higher-order shear deformation theories satisfy the stress-free boundary conditions by offering non-linear variation of shear strains through the height of the cross section. Hence, no shear correction factor is required (Zenkour 2005, Zenkour 2005, El Meiche *et al.* 2011, Merdaci *et al.* 2011, Fahsi *et al.* 2012, Natarajan and Manickam 2012, Sobhy 2013, Nguyen *et al.* 2014, Thai *et al.* 2014). In the preceding studies, the cross-section of the beam is considered to be prismatic. So the effects of variable cross-section along the length of the beam have been ignored.

In light of the aforementioned pints, many researches have been carried out regarding the static analysis of sandwich beams. In the recent years, several researchers have explored different impacts of geometry and material on the behavior of sandwich beams. Among them, Xiang et al. employed finite element method to examine the effects of blast loads on the responses of sandwich beams. Their results were validated through an experimental study (Xiang *et al.* 2016). Moreover, finite element method was used by Kahya for buckling analysis of laminated and sandwich beams. He proposed a laminated beam element. It should be added that delamination and slipping effects were ignored in his research (Kahya 2016). On the other hand, an analytical solution was presented for dynamic analysis of clamped sandwich beams having thick weak cores under a central impact by Liu *et al.* (Liu *et al*. 2017). In 2017, a finite element model was developed for linear elastic analysis of the sandwich beams subjected to severe boundary conditions by Panteghini and

Bardella (2017).

Functionally graded materials (FGM) are a novel generation of composites in which the material properties are allowed to vary from a point to point. It is obvious that FGMs are used in different engineering applications, including aerospace structures, engine combustion chambers, structural elements in micro/nano-electromechanical systems, fusion energy devices and etc. A great variety of potential applications are offered by FGMS in different engineering fields. FGMs are being increasingly used as the constituent material of structural elements, including beams, plates and shells. Numerous researches have been implemented pertaining to the behavior of FG beams. Among them, Davoodinik and Rahimi studied large deflection behavior of tapered FG beams. They introduced a curvilinear coordinates to simplify their nonlinear equations (Davoodinik and Rahimi 2011). Some other researches were also performed about nonlinear behavior of tapered FG beams subjected to different types of loads (Nguyen and Gan 2014, Niknam *et al.* 2014). Further, an analytical solution was presented for static analysis of FG beams with variable cross-section by Nguyen *et al.* They developed their formulations for axially or transversely variation of elastic modulus (Nguyen *et al.* 2014). Also, a new finite element method was employed by Li et al. to investigate static and free vibration analysis of FG tapered beams in which the elastic modulus varied through the thickness and the axial direction (Li *et al.* 2013). Moreover, transient and free vibration analyses of tapered FG Timoshenko beams were studied (Rajasekaran 2013, Calim 2016).

Recently, static and dynamic analysis of FG sandwich beams has widely attracted the attention of researchers. In general, two major types of FG sandwich beams include FG faces-isotropic core and isotropic faces-FG core. Many studies have been dedicated to the behavior of FG sandwich beams, plates and shells. Among them, the research of Venkataraman and Sankar is of significant importance. In this study, they presented elastic theory for stress analysis of sandwich beams with FG core (Venkataraman and Sankar 2003). Moreover, free vibration analysis of FG beams using Rayleigh-Ritz method was investigated by Pradhan and Chakraverty. They developed their formulations within the framework of two theories, including EBBT and TBT (Pradhan and Chakraverty 2013).

In 2015, Filippi *et al*. developed the static analysis of FG beams based on different theories using the finite-element method. Carrera Unified Formulation (CUF) was employed in their study (Filippi *et al.* 2015). Besides, CUF was implemented for free vibration analysis of FG layered beams by Mahat et al. They also utilized finite element method in their research (Mashat *et al.* 2014). Based on the third-order shear deformation theory (TSDT), a quasi-3D model was presented by Vo *et al.* for buckling and free vibration analysis of FG sandwich beams. They applied the finite element method for verification purposes (Vo *et al.* 2015). Furthermore, Ai and Weaver proposed a simplified analytical theory for non-prismatic sandwich beams in which the core material stiffness was variable. In their research, the faces and core of the sandwich beams were modeled based on the Euler-Bernoulli beam and first-order shear deformation theories, respectively (Ai and Weaver 2017). Moreover, a trigonometric higher-order theory of the beam was also presented by Bourada et al. They investigated bending and vibration of FG beams (Bourada *et al*. 2015). Further researches corresponding to analysis of FG beams are available in (Masoodi and Moghaddam 2015, Thai *et al.* 2015, Rezaiee-Pajand and Hozhabrossadati 2016, Rezaiee-Pajand and Masoodi 2016, Shafiei *et al*. 2016, Banić *et al*. 2017, Rezaiee-Pajand *et al.* 2017, Shafiei and Kazemi 2017, Tornabene *et al.* 2017, Tornabene *et al.* 2017, Zare Jouneghani *et al.* 2017).

A survey in the literature reveals that the number of works regarding to the analysis of tapered

FG beams are very limited. However, to the best of the authors' knowledge, there are no reported works on static analysis of FG tapered **sandwich** structures. Owing to this fact, consideration is given to the static behavior of FG tapered FG tapered beams having **sandwich** cross sections the present study for the first time. Variation of the cross-section height is assumed to be linear across the length of the beam. Chebyshev polynomials will be used as auxiliary shape functions. It should be mentioned that the authors' scheme is based on two well-known Timoshenko and Reddy beam theories. Several numerical examples are included in graphical and tabulated forms to show the validity and accuracy of the proposed formulations. For practical purposes, not only the bending and shear stress pushover curves are reported, but also the maximum displacements and stresses are obtained for two types of sandwich beams having different characteristics. In this context, the effects of various factors on static responses of FG tapered sandwich beams are exhaustively investigated.

2. Assumptions

In order to investigate the behavior of a loaded structural member, it is inevitable to consider some simplifying assumptions. Previous researches revealed that the results obtained via Euler-Bernoulli beam theory are not as accurate as those achieved by the higher-order theories, especially, in case of thick and tapered beams. Owing to this fact, Timoshenko and Reddy beam theories, which take the shear effects into account and thus lead to more reliable results, are invoked in the present study. Moreover, since there are no abrupt changes in the mechanical properties of the material constituents at core/face-sheet interfaces, the continuity conditions are satisfied. Hence, the formulation will be based on the single-layer equivalent theory. In order to avoid coupling effects, the non-linear effects are neglected and the cross sections of the beams are considered to be symmetric.

3. Material properties

The non-prismatic FG sandwich beams under consideration are shown in Fig. 1. According to this figure, L is the beam length, $2h_0$ is the core height at the left end of the beam, $2h_1$ denotes the core height at the right end of the beam and $2h(x)$ stands for the core height at any distance from the x origin. Note that h_f and b represent the thickness of the facings and the width of the beam, respectively.

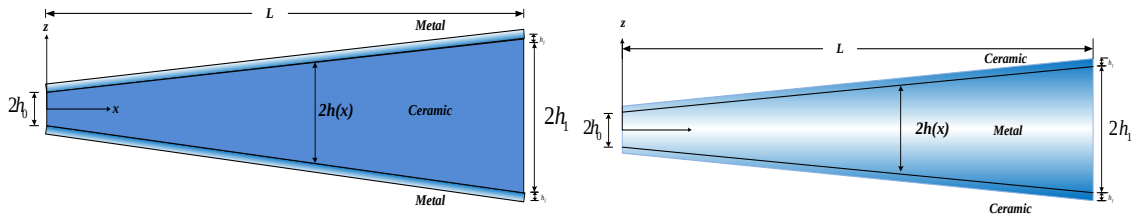

(a) Type (I) (b) Type (II)

Fig. 1 Tapered functionally graded sandwich beams

Beam type (I): Tapered sandwich beam with homogenous core and FG facings

As depicted in Fig. 1(a), beam type (I) is composed of a ceramic core and functionally graded facings. The facing material gradually varies from ceramic at the interfaces to metal at the free edge. The variation of elastic modulus in the face-sheets is given by

$$E(z) = (E_c - E_m)V_c(x, z_k) + E_m \tag{1}$$

where E_c and E_m refer to the elastic modulus of ceramic and metal constituents, respectively. Note that the *z* coordinate is divided into three local coordinates. These local coordinates are denoted by $z_k (k = 1,2,3)$ where z_1, z_2 and z_3 correspond to the bottom facing, the core part and the top facing, respectively. Also, $V_c(x, z_k)$ is the volume fraction of ceramic phase, which is defined as

$$V_c(x, z_k) = \begin{cases} \left(\dfrac{z_3 - \left(h(x) + h_f\right)}{-h_f}\right)^p & for \quad z_3 \in [h(x), h(x) + h_f] \\ 1 & for \quad z_2 \in [-h(x), h(x)] \\ \left(\dfrac{z_1 + h(x) + h_f}{h_f}\right)^p & for \quad z_1 \in [-h(x) - h_f, -h(x)] \end{cases} \tag{2}$$

Beam type (II): Tapered sandwich beam with FG core and homogenous facings According to Fig. 1(b), the core of this beam type is symmetrically functionally graded about the mid-plane of the cross section. Meanwhile, the face-sheets are composed of ceramic. The variation of elastic modulus is expressed by

$$E(z) = (E_m - E_c)V_m(x, z_k) + E_c \tag{3}$$

In the last equation, $V_m(x, z_k)$ refers to the volume fraction of the metal phase and is given by

$$V_m(x, z_k) = \begin{cases} 0 & for \quad z_3 \in [h(x), h(x) + h_f] \\ \left(1 - \left|\dfrac{z_2}{h(x)}\right|\right)^p & for \quad z_2 \in [-h(x), h(x)] \\ 0 & for \quad z_1 \in [-h(x) - h_f, -h(x)] \end{cases} \tag{4}$$

In Eqs. (2) and (4), $p \geq 0$ corresponds to the gradient index. This exponent dictates the rate of material gradation through the beam height. It is obvious that $p = 0$ denotes a homogenous material.

4. Geometry and Kinematics

Clearly, it is difficult and rather impractical to fabricate and bond curved facings and cores in a tapered sandwich beam. For this reason, the core height is assumed to vary linearly along the *x* direction. Consider Fig. 2, which shows the general configuration of a non-prismatic sandwich beam. As it can be seen, upper and lower points of the core at the left end of the beam converge at

point *a*, which is located in a distance designated by ξ. Hereinafter, ξ is referred to as the convergence distance.

If one places the *x* origin at point ***a*** **,**which is used to define the function of the variation of the cross-sectional height, the variation of core height will be given by a function of *x* and ξ as follows

$$h(x) = h_0(\frac{x}{\xi}), x \in [\xi, L+\xi] \tag{5}$$

In order to calculate ξ, the taper ratio parameter is defined as $\lambda = \frac{h_1}{h_0}$. Using the taper ratio relation, ξ will be obtained as

$$\xi = \frac{L}{\lambda - 1} \tag{6}$$

By means Eq. (6), one will be able to obtain the convergence distance for any arbitrary taper ratio. It is important to note that in case of a prismatic member, λ must be set to 1. This makes Eq. (6) to become meaningless. Hence, point a must be theoretically placed at $\xi = \infty$. In such a case, a prismatic member will be defined by Eq. (5) based on the following procedure

$$h_1 = \lim_{\xi \to \infty} h_0 \frac{L+\xi}{\xi} = \lim_{\xi \to \infty} h_0 (1 + \frac{L}{\xi}) = h_0 \tag{7}$$

The displacement field under general beam theory is expressed as (Simsek 2010)

$$\begin{cases} u(x,z) = u_0(x) - z\dfrac{dw_0}{dx} + \Phi(x,z)\eta_0(x) \\ w(x,z) = w_0(x) \end{cases} \tag{8}$$

where u_0 and w_0 represent the longitudinal and transverse displacements of the mid-plane, respectively. Also, η_0 denotes the shear strain on the mid-plane and is given by

$$\eta_0(x) = \frac{dw_0(x)}{dx} + \psi(x) \tag{9}$$

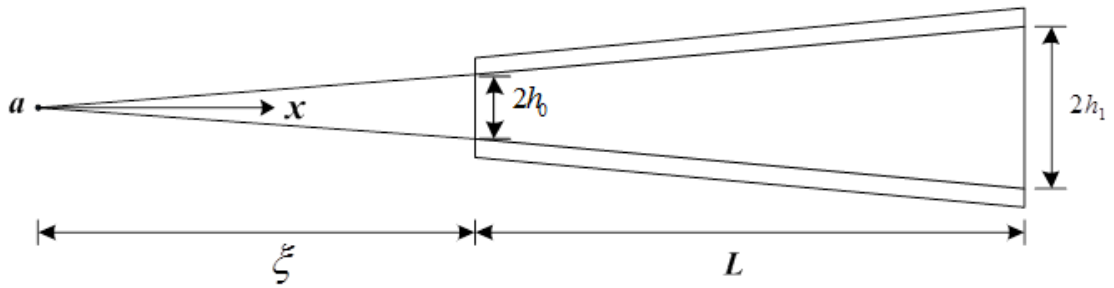

Fig. 2 Geometry of a tapered sandwich beam

in which $\psi(x)$ corresponds to the rotation of the cross section about the mid-plane of the beam. In addition, $\Phi(x,z)$ is a function which determines the variation of shear strains along the height of the cross section. In case of a prismatic member, Φ will be only a function of z. A variety of shear deformation theories will be attained by choosing proper expressions for $\Phi(x,z)$. Based on the TBT and RBT, and in case of a non-prismatic member, $\Phi(x,z)$ can be defined as

$$\begin{aligned} &\text{TBT: } \Phi(x,z) = z \\ &\text{RBT: } \Phi(x,z) = z\left(1 - \frac{z^2}{3\left(h(x)+h_f\right)^2}\right) \end{aligned} \tag{10}$$

Based on the foregoing definitions, the non-zero strains will be expressed by

$$\begin{aligned} \varepsilon_x &= \frac{\partial u}{\partial x} = u_{0,x} - z w_{0,xx} + \Phi \eta_{0,x} + \Phi_{,x}\eta_0 \\ \gamma_{xz} &= \frac{\partial u}{\partial z} + \frac{\partial w}{\partial x} = \Phi_{,z}\eta_0 \end{aligned} \tag{11}$$

where the subscript (,) indicates differentiation with respect to coordinates. In the present study, u_0 is set to zero due to symmetry. Based on the plane stress conditions and assuming that the material of the tapered beams follows Hooke's law, the stress-strain relationships are given by (Vo *et al.* 2015)

$$\begin{aligned} \sigma_x &= E(z)\varepsilon_x \\ \tau_{xz} &= G(z)\gamma_{xz} \end{aligned} \tag{12}$$

where $G(z) = \frac{E(z)}{2(1+\nu)}$ refers to the shear modulus and ν is the Poisson's ratio.

5. Problem formulation and solution procedure

The strain energy of the structure is given by

$$U = \frac{1}{2}\int_\Omega \left(\sigma_x\varepsilon_x + k_s\tau_{xz}\gamma_{xz}\right)d\Omega = \frac{1}{2}b\int_L \sum_{k=1}^{3}\int_{z_k}\left(\sigma_x^{(k)}\varepsilon_x + k_s\tau_{xz}^{(k)}\gamma_{xz}\right)dz_k \tag{13}$$

where Ω denotes the beam domain on which the integration must be carried out and k_s is the shear correction factor. In the TBT formulation, k_s equals to $\frac{5}{6}$ for isotropic homogenous rectangular cross sections. On the other hand, a shear correction factor is not required for the RBT since the stress-free boundary conditions are satisfied. Upon substitution for strains and stresses from Eqs. (11) and (12) into Eq. (13), one arrives at the following weak form statement

$$\begin{aligned} U = \frac{1}{2}\int_L \Big\{ &\left(A_{xx} + k_s A_{xz}\right)\left(w_{0,x}^2 + 2w_{0,x}\psi + \psi^2\right) - 2\left(w_{0,x}+\psi\right)\left[B_{xx}w_{0,xx} + E_{xx}\left(w_{0,xx}+\psi_{,x}\right)\right] \\ &+ D_{xx}w_{0,xx}^2 - 2F_{xx}w_{0,xx}\left(w_{0,xx}+\psi_{,x}\right) + H_{xx}\left(w_{0,xx}^2 + 2w_{0,xx}\psi_{,x} + \psi_{,x}^2\right)\Big\}dx \end{aligned} \tag{14}$$

where the subsequent stiffness coefficients are used

$$\begin{aligned}
\left(A_{xx}, B_{xx}\right) &= b\sum_{k=1}^{3}\int_{z_k} E(z_k)\Phi_{,x}(\Phi_{,x}, z_i)\,dz_k \\
\left(E_{xx}, F_{xx}\right) &= b\sum_{k=1}^{3}\int_{z_k} E(z_k)\Phi(\Phi_{,x}, z_k)\,dz_k \\
H_{xx} &= b\sum_{k=1}^{3}\int_{z_k} E(z_k)\Phi^2 dz_k \\
A_{xz} &= b\sum_{k=1}^{3}\int_{z_k} G(z_k)\left(\Phi_{,z}\right)^2 dz_k
\end{aligned} \tag{15}$$

It is important to note that the coefficients outlined in Eq. (15) are functions of x for non-prismatic sections. In this study, it is assumed that the beam is subjected to a transversely distributed load. The external potential energy exerted by the distributed load $q(x)$ is defined as

$$V = \int_L q(x) w_0 dx \tag{16}$$

The total potential energy can be obtained as

$$\Pi = U - V \tag{17}$$

Based on the Ritz method, the unknown functions $\psi(x)$ and $w_0(x)$ must be approximated in such a way that satisfies the essential boundary conditions. Improper shape functions may reduce the rate of convergence and lead to numerical instabilities. However, Lagrangian multipliers can be applied for shape functions which do not satisfy the boundary conditions (Nguyen *et al.* 2017). In the present study, Chebyshev polynomials of the first kind are invoked as the auxiliary shape functions. It will be later shown that the exceptional orthogonality of these polynomials results in a significant convergence rate. Generally, the range of these orthogonal polynomials is $R=[-1,1]$ on the domain of the beam length, that is $x \in [\xi, L+\xi]$. The shifted Chebyshev polynomials are expressed by

$$T_n(\mu) = \cos\left(\frac{\pi n}{2}\right) + n\sum_{j=1}^{n}\frac{(\mu)^j}{2j}\cos\left(\frac{\pi(n-j)}{2}\right)\binom{\frac{n+j-2}{2}}{j-1} \tag{18}$$

where $\mu = \dfrac{2(x-\xi)}{L} - 1$ is the shifted coordinate. Making use of Eq. (18), unknown displacement functions are assumed in the following approximate form

$$\begin{aligned}
w_0(x) &= \sum_{n=0}^{N} w_n f_n(x), \qquad f_n(x) = T_n(\mu)\alpha(x) \\
\psi(x) &= \sum_{n=0}^{N} \psi_n g_n(x), \qquad g_n(x) = T_n(\mu)\beta(x)
\end{aligned} \tag{19}$$

Table 1 The values of shape function powers

Boundary Conditions	$x=\xi$		$x=L+\xi$	
	p_1	p_2	p_3	p_4
Pinned-Pinned	1	1	0	0
Clamped-Clamped	2	2	1	1
Free-Clamped	0	2	0	1

In Eq. (19), w_n and ψ_n are unknown constants to be determined and N is the number of selected terms. Also, $\alpha(x)$ and $\beta(x)$, which depend on the boundary conditions, are defined as

$$\alpha(x)=\left(\frac{x-\xi}{L}\right)^{p_1}\left(1-\frac{x-\xi}{L}\right)^{p_2}$$
$$\beta(x)=\left(\frac{x-\xi}{L}\right)^{p_3}\left(1-\frac{x-\xi}{L}\right)^{p_4} \tag{20}$$

The values of powers p_1 to p_4 are proposed in Table 1 for various conventional boundary conditions. As it is well-known, application of the principle of minimum total potential energy yields

$$\frac{\partial \Pi}{\partial w_n}=0,\frac{\partial \Pi}{\partial \psi_n}=0,n=0,1,...,N \tag{21}$$

To obtain the system of governing equations, Eq. (19) is inserted into Eq. (14) and the subsequent expression is substituted into Eq. (17). Then, by introducing the resulting expression for the total potential energy into Eq. (21), one arrives at the following system of linear algebraic equations

$$[S]\{D\}=\{Q\} \tag{22}$$

where S, D and Q refer to the coefficients matrix, displacements vector and load vector, respectively. Eq. (22) can be further expanded as

$$\begin{bmatrix}[S_{11}] & [S_{12}]\\ sym & [S_{22}]\end{bmatrix}\begin{Bmatrix}\{w\}\\ \{\psi\}\end{Bmatrix}=\begin{Bmatrix}\{Q\}\\ 0\end{Bmatrix} \tag{23}$$

The components of the coefficients matrix and the load vector of Eq. (23) are explicitly obtained as

$$S_{11}(i,j)=\int_L\left[\left(A_1 f_{j,xx}+A_2 f_{j,x}\right)f_{i,xx}+\left(A_2 f_{j,xx}+A_3 f_{j,x}\right)f_{i,x}\right]dx$$
$$S_{12}(i,j)=\int_L\left[\left(A_4 g_{j,x}+A_2 g_j\right)f_{i,xx}+\left(E_{xx} g_{j,x}+A_3 g_j\right)f_{i,x}\right]dx$$
$$S_{22}(i,j)=\int_L\left[\left(H_{xx} g_{j,x}+E_{xx} g_j\right)g_{i,x}+\left(E_{xx} g_{j,x}+A_3 g_j\right)g_i\right]dx$$
$$Q_i=\int_L f_i\,dx \tag{24}$$

where $A_1 = D_{xx} - 2F_{xx} + H_{xx}$, $A_2 = E_{xx} - B_{xx}$, $A_3 = k_s A_{xz} + A_{xx}$ and $A_4 = H_{xx} - F_{xx}$. Further, i and j refer to the row number and the column number of the submatrices, respectively. Solving the system of equations given by Eq. (23) simultaneously results in the unknown coefficients.

6. Numerical results

In this section, verification and comparative studies are carried out to illustrate the accuracy of the proposed scheme for prismatic members. Furthermore, the effects of taper ratio, gradient index and beam length to the depth ratio on deflections, and stresses are investigated. Various cross sectional types for sandwich beams are considered. Each of these cross sections indicates specific core height to face-sheet thickness ratios at $x = \xi$. For example, in 1-8-1 cross section, the core height at $x = \xi$ is 8 times greater than the thickness facings while the thicknesses of the face-sheets are identical. Hereinafter, F, C and S indicate free, clamped and simple boundary conditions. In all cases, Alumina with E_c = 380 GPa and ν = 0.3 is considered as the ceramic constituent while Aluminum, with E_m = 70 GPa and ν = 0.3 consists the metal phase. For the sake of simplicity and generality, maximum deflection, bending and shear stresses will be reported in the following normalized form

$$w^*_{max} = \frac{100 E_m H^3 w_{max}}{q_0 L^4}$$
$$\sigma^*_x(x,z) = \frac{\sigma(x,z) H}{q_0 L}$$
$$\tau^*_{xz}(x,z) = \frac{\tau(x,z) H}{q_0 L} \tag{25}$$

Note that q_0 indicates the intensity of the uniform distributed load and $H = 2(h(\xi) + h_f)$ corresponds to the total height of the cross section at $x = \xi + L$.

6.1 Tapered sandwich beam type (I)

This example is dedicated to the static analysis of beam type (I). Maximum deflections of a prismatic beam type (I) ($\lambda = 1$) with two cross sectional types of 1-1-1 and 1-2-1 are compared with the results presented by Vo *et al.* (2015) in Table 2. There is excellent agreement between the present results obtained by Chebyshev polynomials, and those obtained by Vo *et al.* Thus, the validity of the proposed scheme is clearly established.

In order to examine the convergence efficiency of the proposed solution procedure, convergence studies for maximum deflections and shear stresses of beam type (I) with 1-2-1 and 2-1-2 cross sections, $\lambda = 2$ and $p = 1$ are carried out in Table 3. To highlight the shear effects, the slenderness ratio is considered as $L/H = 5$. As it can be seen, Chebyshev polynomials bear a remarkable rate of convergence. Stable responses are likely to be achieved by selecting 6 or 8 terms in the series solution. In the problems to be presented below, 10 terms in the series solution would be sufficient to assure negligible error.

Table 2 Comparison study of the maximum deflections for a prismatic beam of type (I)

L/H	p	Theory	Boundary Conditions					
			S-S		C-C		F-C	
			1-1-1	1-2-1	1-1-1	1-2-1	1-1-1	1-2-1
5	0	FSDT (Vo *et al.* 2015)	3.1657	3.1657	0.8630	0.8630	28.7811	28.7811
		TSDT (Vo *et al.* 2015)	3.1654	3.1654	0.8501	0.8501	28.7555	28.7555
		Present TBT	3.1657	3.1657	0.8631	0.8630	28.7811	28.7811
		Present RBT	3.1653	3.1654	0.8501	0.8501	28.7555	28.7555
	1	FSDT (Vo *et al.* 2015)	6.3128	5.4408	1.5783	1.3770	58.3924	50.2103
		TSDT (Vo *et al*. 2015)	6.2693	5.4122	1.5232	1.3372	58.1959	50.0741
		Present TBT	6.3128	5.4407	1.5783	1.3770	58.3924	50.2103
		Present RBT	6.2693	5.4122	1.5233	1.3373	58.1959	50.0741
	2	FSDT (Vo *et al.* 2015)	8.4582	6.8003	2.0523	1.6758	78.6742	63.0722
		TSDT (Vo *et al*. 2015)	8.3893	6.7579	1.9715	1.6225	78.3753	62.8813
		Present TBT	8.4582	6.8003	2.0523	1.6758	78.6742	63.0722
		Present RBT	8.3893	6.7580	1.9715	1.6225	78.3753	62.8813
	5	FSDT (Vo *et al.* 2015)	11.3372	8.5762	2.6879	2.0635	105.8940	79.8939
		TSDT (Vo *et al.* 2015)	11.2274	8.5137	2.5652	1.9896	105.4300	79.6213
		Present TBT	11.3372	8.5764	2.6879	2.0635	105.8940	79.8939
		Present RBT	11.2273	8.5137	2.5652	1.9896	105.4300	79.6213
20	0	FSDT (Vo *et al.* 2015)	2.8963	2.8963	0.5936	0.5936	27.7034	27.7034
		TSDT (Vo *et al.* 2015)	2.8963	2.8963	0.5933	0.5933	27.7029	27.7029
		Present TBT	2.8965	2.8963	0.5936	0.5936	27.7034	27.7034
		Present RBT	2.8963	2.8963	0.5933	0.5933	27.7029	27.7029
	1	FSDT (Vo *et al.* 2015)	5.9428	5.1024	1.2083	1.0385	56.9123	48.8566
		TSDT (Vo *et al*. 2015)	5.9401	5.1006	1.2053	1.0365	56.9009	48.8489
		Present TBT	5.9428	5.1024	1.2083	1.0385	56.9123	48.8566
		Present RBT	5.9401	5.1006	1.2053	1.0365	56.9009	48.8489
	2	FSDT (Vo *et al.* 2015)	8.0356	6.4302	1.6297	1.3058	76.9836	61.5921
		TSDT (Vo *et al.* 2015)	8.0313	6.4276	1.6250	1.3028	76.9658	61.5809
		Present TBT	8.0356	6.4302	1.6297	1.3058	76.9836	61.5921
		Present RBT	8.0312	6.4276	1.6250	1.3028	76.9658	61.5809
	5	FSDT (Vo *et al.* 2015)	10.8445	8.1681	2.1952	1.6554	103.9230	78.2614
		TSDT (Vo *et al.* 2015)	10.8376	8.1642	2.1880	1.6512	103.8950	78.2451
		Present TBT	10.8445	8.1681	2.1952	1.6554	103.9230	78.2614
		Present RBT	10.8376	8.1642	2.1880	1.6512	103.8950	78.2451

Table 3 Convergence of normalized maximum deflections and shear stresses for a simply supported tapered FG beam type (I)

No. of terms (N)	1.2.1				2.1.2			
	TBT		RBT		TBT		RBT	
	$w^*_{\max}$	$\tau^*_{xz}(\xi,0)$	$w^*_{\max}$	$\tau^*_{xz}(\xi,0)$	$w^*_{\max}$	$\tau^*_{xz}(\xi,0)$	$w^*_{\max}$	$\tau^*_{xz}(\xi,0)$
1	2.0670	0.7358	2.0701	0.9391	4.0647	0.8846	4.0261	0.9956
2	2.3762	0.7512	2.3883	0.5811	4.2054	0.8901	4.2211	0.5622
3	2.6860	0.7533	2.6745	0.6837	5.0645	0.8905	5.0219	0.8358
4	2.7456	0.7536	2.7226	0.7757	5.0944	0.8906	5.0477	0.9093
5	2.7417	0.7537	2.7205	0.8075	5.0912	0.8906	5.0454	0.9194
6	2.7410	0.7537	2.7202	0.8124	5.0912	0.8906	5.0455	0.9176
7	2.7410	0.7537	2.7203	0.8096	5.0912	0.8906	5.0455	0.9166
8	2.7410	0.7537	2.7203	0.8077	5.0912	0.8906	5.0455	0.9166
9	2.7410	0.7537	2.7203	0.8077	5.0912	0.8906	5.0455	0.9166
10	2.7410	0.7537	2.7203	0.8077	5.0912	0.8906	5.0455	0.9166

Tables 4-6 are presented to show the maximum dimensionless deflections of beam type (I) with various boundary conditions, cross sectional types, gradient indexes and taper ratios. Length to depth ratios are selected 5 and 20 to underscore the shear effects. Clearly, the maximum deflection in prismatic CC and SS beams occurs at mid span, i.e., $x = \xi + \frac{L}{2}$. In contrary, various factors, including taper ratio, elastic modulus variation and cross sectional types change the location of this point in tapered beams. As it is expected, an increment in taper ratio results in smaller maximum deflections. In addition, similar to prismatic beams, the maximum deflection obtained via RBT is smaller than that obtained by TBT.

It is also seen that for $L/H = 5$, which indicates a thick beam, the difference between TBT and RBT results is more significant than the difference observed in slender beams with $L/H = 20$. Insomuch as the shear effects do not require a correction factor in RBT, this theory results in more accurate deflections and the difference between TBT and RBT responses relatively increase as λ is amplified and L/H is decreased. These facts demonstrate the importance of shear effects in thick beams. Another important result is that the maximum deflection of type (I) beam, with a given taper ratio, increases as the gradient index is increased. This takes place due to the decrease in the volume fraction of ceramic phase in the face-sheets which eventually leads to a decrease in the flexural stiffness of the beam.

Considering various factors, the maximum non-dimensional shear stresses for a simply supported beam type (I) are outlined in Table 7. As it could be predicted, the maximum shear stress is not influenced by variation of the taper ratio. This is owing to the fact that a simply supported beam is always determinate and the support reactions are not influenced by chaning the taper ratio. Morever, an increase in gradient index results in higher shear stresses.

Table 4 Maximum dimensionless deflections of beam type (I) with SS supports

p	λ	Theory	*L*/*H*=5				*L*/*H*=20			
			1-1-1	1-2-1	1-8-1	2-1-2	1-1-1	1-2-1	1-8-1	2-1-2
0	1.5	TBT	2.5416	2.3007	1.9503	2.7653	2.2922	2.0594	1.7219	2.5084
		RBT	2.5408	2.2993	1.9478	2.7649	2.2921	2.0594	1.7218	2.5083
	2	TBT	2.0946	1.7622	1.3447	2.4406	1.8607	1.5412	1.1420	2.1945
		RBT	2.0925	1.7587	1.3385	2.4397	1.8607	1.5412	1.1417	2.1944
	3	TBT	1.5078	1.1491	0.7770	1.9503	1.2976	0.9562	0.6062	1.7219
		RBT	1.5029	1.1411	0.7642	1.9478	1.2974	0.9558	0.6055	1.7218
1	1.5	TBT	4.8409	3.7363	2.3561	5.9257	4.5068	3.4404	2.1103	5.5523
		RBT	4.8039	3.7135	2.3500	5.8764	4.5045	3.4391	2.1099	5.5493
	2	TBT	3.8381	2.7410	1.5844	5.0912	3.5304	2.4741	1.3678	4.7394
		RBT	3.8051	2.7202	1.5758	5.0455	3.5287	2.4728	1.3673	4.7365
	3	TBT	2.5974	1.6794	0.8869	3.8809	2.3271	1.4503	0.7055	3.5623
		RBT	2.5677	1.6587	0.8727	3.8401	2.3252	1.4491	0.7047	3.5597
2	1.5	TBT	6.3551	4.5507	2.5234	8.1918	5.9782	4.2307	2.2713	7.7519
		RBT	6.2978	4.5181	2.5161	8.1104	5.9747	4.2289	2.2709	7.7468
	2	TBT	4.9519	3.2751	1.6811	6.9623	4.6077	2.9881	1.4593	6.5515
		RBT	4.9021	3.2465	1.6715	6.8881	4.6052	2.9863	1.4587	6.5468
	3	TBT	3.2596	1.9533	0.9300	5.2032	2.9600	1.7086	0.7446	4.8356
		RBT	3.2169	1.9271	0.9153	5.1388	2.9576	1.7070	0.7438	4.8316
5	1.5	TBT	8.3860	5.5926	2.7073	11.1647	7.9538	5.2440	2.4485	10.6293
		RBT	8.2967	5.5457	2.6984	11.0297	7.9484	5.2413	2.4479	10.6209
	2	TBT	6.4376	3.9468	1.7861	9.4430	6.0470	3.6364	1.5589	8.9490
		RBT	6.3616	3.9071	1.7753	9.3214	6.0430	3.6339	1.5582	8.9414
	3	TBT	4.1307	2.2894	0.9764	6.9727	3.7946	2.0266	0.7870	6.5374
		RBT	4.0681	2.2551	0.9607	6.8695	3.7907	2.0245	0.7860	6.5310

Fig. 3 is presented to illustrate the variation of $\tau_{xz}^{*}(\xi,0)$ obtained via RBT for a simply supported beam with various cross sectional types. As it is seen in this figure, the maximum shear stress, which occurs at the mid-surface, increases by increasing the value of gradient index. Another interesting result is that for a given cross section, the effect of gradient index on the maximum shear stress is hardly significant. This happens because the height of the cross section, and the support reaction at $x=\xi$ remain constant irrespective of the taper ratio.

Table 5 Maximum dimensionless deflections of beam type (I) with CC supports

p	λ	Theory	*L*/*H*=5				*L*/*H*=20			
			1-1-1	1-2-1	1-8-1	2-1-2	1-1-1	1-2-1	1-8-1	2-1-2
0	1.5	TBT	0.7087	0.6534	0.5718	0.7596	0.4708	0.4236	0.3551	0.5145
		RBT	0.7069	0.6475	0.5653	0.7569	0.4708	0.4234	0.3551	0.5145
	2	TBT	0.6055	0.5274	0.4266	0.6856	0.3833	0.3184	0.2371	0.4511
		RBT	0.5994	0.5203	0.4177	0.6800	0.3832	0.3183	0.2370	0.4508
	3	TBT	0.4664	0.3777	0.2809	0.5718	0.2688	0.1992	0.1275	0.3551
		RBT	0.4584	0.3683	0.2686	0.5653	0.2687	0.1989	0.1272	0.3551
1	1.5	TBT	1.2354	0.9831	0.6662	1.4847	0.9172	0.7018	0.4334	1.1287
		RBT	1.1981	0.9579	0.6572	1.4364	0.9152	0.7004	0.4331	1.1234
	2	TBT	1.0103	0.7569	0.4844	1.2984	0.7191	0.5057	0.2824	0.9639
		RBT	0.9759	0.7351	0.4740	1.2512	0.7171	0.5046	0.2821	0.9611
	3	TBT	0.7257	0.5068	0.3091	1.0246	0.4744	0.2975	0.1473	0.7245
		RBT	0.6969	0.4873	0.2959	0.9838	0.4729	0.2965	0.1468	0.7222
2	1.5	TBT	1.5714	1.1644	0.7045	1.9906	1.2128	0.8605	0.4658	1.5713
		RBT	1.5158	1.1302	0.6946	1.9115	1.2091	0.8585	0.4653	1.5658
	2	TBT	1.2594	0.8778	0.5072	1.7174	0.9345	0.6084	0.3007	1.3275
		RBT	1.2096	0.8492	0.4963	1.6422	0.9315	0.6068	0.3004	1.3229
	3	TBT	0.8759	0.5706	0.3198	1.3224	0.5994	0.3484	0.1551	0.9777
		RBT	0.8362	0.5466	0.3063	1.2603	0.5972	0.3472	0.1545	0.9741
5	1.5	TBT	2.0197	1.3943	0.7464	2.6601	1.6089	1.0635	0.5014	2.1502
		RBT	1.9338	1.3466	0.7352	2.5307	1.6039	1.0607	0.5009	2.1432
	2	TBT	1.5884	1.0279	0.5319	2.2751	1.2207	0.7373	0.3207	1.8072
		RBT	1.5142	0.9893	0.5202	2.1548	1.2162	0.7351	0.3203	1.7999
	3	TBT	1.0699	0.6474	0.3313	1.7183	0.7621	0.4106	0.1634	1.3129
		RBT	1.0133	0.6170	0.3173	1.6216	0.7589	0.4089	0.1628	1.3071

It is also important to note that regardless of the effects of taper ratio and cross sectional types, an increment in the gradient index decreases the shear stress in the face-sheets. As the ratio of the face-sheet thicknesses to the core height increases, the effects of the volume fraction of metal constituent gain importance. Hence, the stiffness of the cross section decreases, which results in larger axial and shear strains. As it can be seen in Table 7 and Fig. 3, this will lead to higher shear stresses. Clearly, in case of a CC beam, increase of taper ratio changes the rigidity of the supports and their reactions. This factor in turn reduces the maximum shear stress along the beam.

Table 6 Maximum dimensionless deflections of beam type (I) with FC supports

p	λ	Theory	*L*/*H*=5				*L*/*H*=20			
			1-1-1	1-2-1	1-8-1	2-1-2	1-1-1	1-2-1	1-8-1	2-1-2
0	1.5	TBT	20.0699	17.0822	13.1097	23.0280	19.1141	16.1702	12.2667	22.0321
		RBT	19.9825	16.9730	12.9687	22.9579	19.1091	16.1639	12.2584	22.0282
	2	TBT	14.6954	11.1643	7.3114	18.7953	13.8196	10.3581	6.6026	17.8542
		RBT	14.5630	11.0050	7.1248	18.6963	13.8118	10.3487	6.5917	17.8484
	3	TBT	8.7389	5.7351	3.1645	13.1150	7.9896	5.0791	2.6260	12.2670
		RBT	8.5611	5.5405	2.9655	12.9687	7.9791	5.0675	2.6142	12.2584
1	1.5	TBT	37.9562	27.3489	15.6574	49.4834	36.7009	26.2427	14.7563	48.0494
		RBT	37.7541	27.1755	15.5113	49.2274	36.6879	26.2322	14.7475	48.0339
	2	TBT	26.2339	16.7888	8.4400	38.7667	25.1034	15.8336	7.6888	37.4413
		RBT	26.0066	16.5881	8.2503	38.5133	25.0895	15.8215	7.6773	37.4257
	3	TBT	14.2623	7.9162	3.5087	25.1901	13.3323	7.1629	2.9459	24.0417
		RBT	14.0273	7.7020	3.3101	24.9277	13.318	7.1500	2.9340	24.0257
2	1.5	TBT	49.5649	33.0273	16.6910	68.3585	48.1451	31.8374	15.7674	66.6768
		RBT	49.2854	32.8255	16.5419	67.9853	48.1278	31.8249	15.7585	66.6538
	2	TBT	33.3487	19.7313	8.8795	52.6408	32.0965	18.7002	8.1150	51.1088
		RBT	33.0719	19.4995	8.6912	52.2871	32.0796	18.6869	8.1038	51.0853
	3	TBT	17.4052	8.9630	3.6384	33.1472	16.3933	8.1703	3.0669	31.8442
		RBT	17.1426	8.7408	3.4400	32.8173	16.3772	8.1569	3.0551	31.8239
5	1.5	TBT	65.0861	40.2064	17.8190	93.2875	63.4672	38.9155	16.8695	91.2542
		RBT	64.6943	39.9596	17.6632	92.7117	63.4440	38.9004	16.8603	91.2183
	2	TBT	42.7409	23.3187	9.3503	71.1892	41.3387	22.2284	8.5729	69.3681
		RBT	42.3886	23.0733	9.1634	70.6764	41.3170	22.2135	8.5616	69.3361
	3	TBT	21.4286	10.2008	3.7751	43.8075	20.3183	9.3641	3.1947	42.3006
		RBT	21.1238	9.9665	3.5766	43.3672	20.2996	9.3498	3.1828	42.2735

Fig. 4 depicts the variation of bending stress through the height of the clamped support of a FC beam with various taper ratios and gradient indexes. In this figure, $H_1 = 2(h(\xi + L) + h_f)$ denotes the total height of the beam at the clamped end, i.e., $x = \xi + L$.

The most important point in Fig. 4 is that when the value of the gradient index is 1, the maximum bending stress occurs at the face-sheets for cross sectional type 2-1-2 in which the facings are thick. In other cases, the maximum bending stress occurs at the core/face interfaces. Thus, in practical cases, the interfaces must be strengthened properly. Moreover, as it can be predicted, for a certain cross sectional type, an increase in taper ratio results in smaller bending stresses.

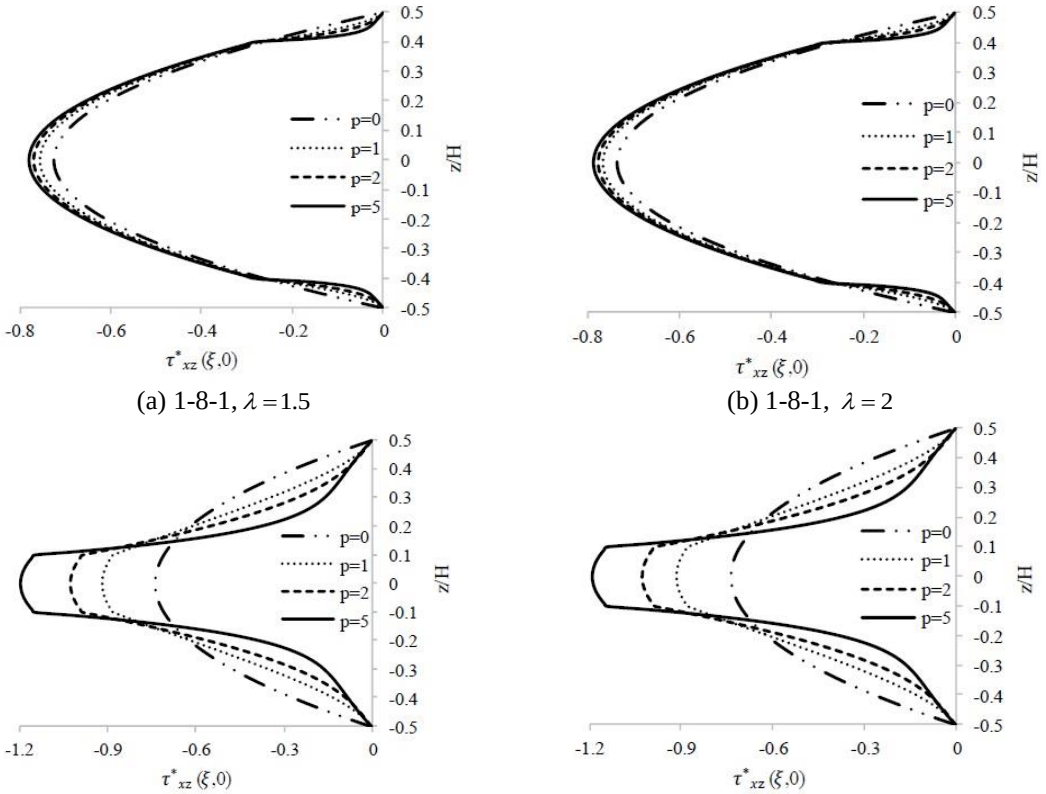

(a) 1-8-1, $\lambda=1.5$ (b) 1-8-1, $\lambda=2$

(c) 2-1-2, $\lambda=1.5$ (d) 2-1-2, $\lambda=2$

Fig. 3 Variation of $\tau^*_{xz}(\xi,z)$ for various cross sectional types in a simply supported beam , $L/H=5$

Table 7 Maximum dimensionless shear stress $\tau^*_{xz}(\xi,0)$ in a simply supported beam type (I)

p	λ	Theory	L/H =5				L/H =20			
			1-1-1	1-2-1	1-8-1	2-1-2	1-1-1	1-2-1	1-8-1	2-1-2
0	1.5	TBT	0.6000	0.6000	0.6000	0.6000	0.6000	0.6000	0.6000	0.6000
		RBT	0.7401	0.7382	0.7336	0.7385	0.7486	0.7473	0.7477	0.7490
	2	TBT	0.6000	0.6000	0.6000	0.6000	0.6000	0.6000	0.6000	0.6000
		RBT	0.7401	0.7382	0.7336	0.7385	0.7486	0.7473	0.7404	0.7490
	3	TBT	0.6000	0.6000	0.6000	0.6000	0.6000	0.6000	0.6000	0.6000
		RBT	0.7401	0.7382	0.7336	0.7385	0.7486	0.7473	0.7314	0.7490
1	1.5	TBT	0.8241	0.7537	0.6532	0.8906	0.8241	0.7537	0.6532	0.8906
		RBT	0.8660	0.8077	0.7643	0.9166	0.8716	0.8232	0.7747	0.9269
	2	TBT	0.8241	0.7537	0.6532	0.8906	0.8241	0.7537	0.6532	0.8906
		RBT	0.8660	0.8077	0.7643	0.9166	0.8716	0.8232	0.7667	0.9269

Continued-

	3	TBT	0.8241	0.7537	0.6532	0.8906	0.8241	0.7537	0.6532	0.8906
		RBT	0.8660	0.8077	0.7643	0.9166	0.8716	0.8232	0.7569	0.9269
2	1.5	TBT	0.9412	0.8241	0.6732	1.0621	0.9412	0.8241	0.6732	1.0621
		RBT	0.9325	0.8544	0.7758	1.0269	0.9379	0.8595	0.7850	1.0350
	2	TBT	0.9412	0.8241	0.6732	1.0621	0.9412	0.8241	0.6732	1.0621
		RBT	0.9325	0.8544	0.7758	1.0269	0.9379	0.8595	0.7850	1.0350
	3	TBT	0.9412	0.8241	0.6732	1.0621	0.9412	0.8241	0.6732	1.0621
		RBT	0.9325	0.8544	0.7758	1.0269	0.9379	0.8595	0.7850	1.0350
5	1.5	TBT	1.0973	0.9089	0.6944	1.3153	1.0973	0.9089	0.6944	1.3153
		RBT	1.0207	0.8974	0.7873	1.1934	1.0265	0.9026	0.7956	1.2027
	2	TBT	1.0973	0.9089	0.6944	1.3153	1.0973	0.9089	0.6944	1.3153
		RBT	1.0207	0.8974	0.7873	1.1934	1.0265	0.9026	0.7956	1.2027
	3	TBT	1.0973	0.9089	0.6944	1.3153	1.0973	0.9089	0.6944	1.3153
		RBT	1.0207	0.8974	0.7873	1.1934	1.0265	0.9026	0.7956	1.2027

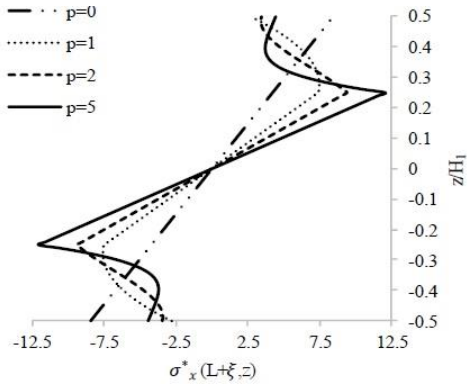

(a) 1-8-1, $\lambda = 1.5$

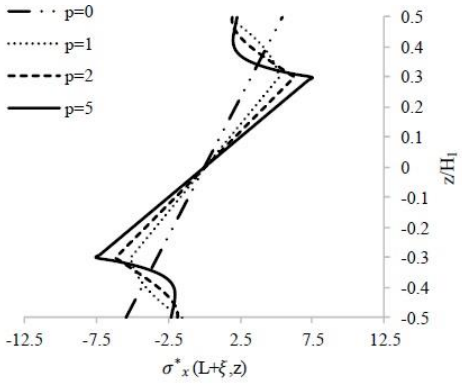

(b) 1-8-1, $\lambda = 2$

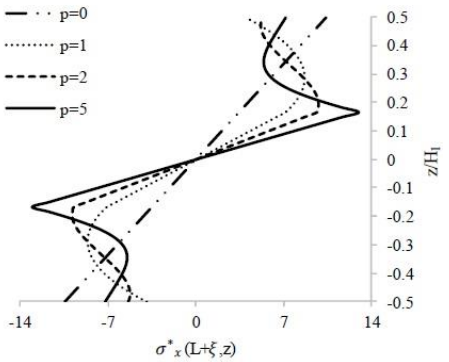

(c) 2-1-2, $\lambda = 1.5$

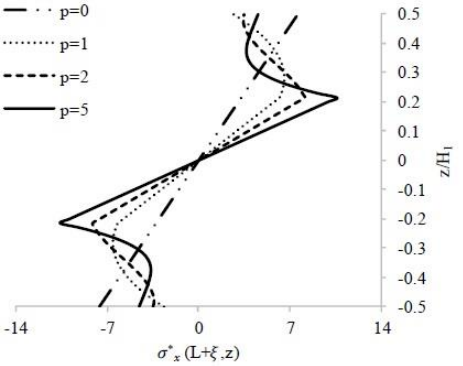

(d) 2-1-2, $\lambda = 2$

Fig. 4 Variation of $\sigma_x^*(L+\xi, z)$ for various cross sectional types in the clamped end of a FC beam, $L/H = 5$

Table 8 Maximum dimensionless deflections of beam type (II) with SS supports

p	λ	Theory	*L*/*H* =5				*L*/*H* =20			
			1-1-1	1-2-1	1-8-1	2-1-2	1-1-1	1-2-1	1-8-1	2-1-2
1	1	TBT	3.2327	3.3145	3.6404	3.1958	2.9209	2.9761	3.2405	2.9025
		RBT	3.2793	3.3917	3.7665	3.2207	2.9239	2.9810	3.2484	2.9041
	1.5	TBT	2.6171	2.4480	2.3005	2.8014	2.3216	2.1370	1.9557	2.5170
		RBT	2.6675	2.5240	2.4055	2.8304	2.3248	2.1418	1.9623	2.5189
	2	TBT	2.1746	1.9030	1.6197	2.4815	1.8930	1.6133	1.3110	2.2054
		RBT	2.2263	1.9742	1.7058	2.5133	1.8963	1.6178	1.3165	2.2074
	3	TBT	1.5909	1.2739	0.9691	1.9983	1.3317	1.0157	0.7064	1.7364
		RBT	1.6404	1.3329	1.0261	2.0332	1.3348	1.0194	0.7101	1.7387
2	1	TBT	3.2030	3.2405	3.3710	3.1840	2.9067	2.9287	3.0267	2.8991
		RBT	3.2307	3.2851	3.4457	3.1994	2.9085	2.9315	3.0314	2.9001
	1.5	TBT	2.5829	2.3745	2.1048	2.7868	2.3045	2.0908	1.8101	2.5123
		RBT	2.6125	2.4178	2.1668	2.8045	2.3064	2.0936	1.8140	2.5134
	2	TBT	2.1378	1.8327	1.4685	2.4640	1.8742	1.5703	1.2057	2.1993
		RBT	2.1674	1.8724	1.5181	2.4836	1.8761	1.5728	1.2089	2.2005
	3	TBT	1.5521	1.2120	0.8668	1.9778	1.3118	0.9801	0.6441	1.7282
		RBT	1.5789	1.2427	0.8968	1.9977	1.3135	0.9821	0.6460	1.7295
5	1	TBT	3.1808	3.1918	3.2223	3.1740	2.8986	2.9028	2.9200	2.8970
		RBT	3.1932	3.2114	3.2553	3.1810	2.8994	2.9040	2.9221	2.8975
	1.5	TBT	2.5581	2.3265	1.9956	2.7749	2.2949	2.0658	1.7382	2.5094
		RBT	2.5709	2.3448	2.0219	2.7828	2.2957	2.0669	1.7399	2.5099
	2	TBT	2.1115	1.7870	1.3829	2.4511	1.8637	1.5471	1.1541	2.1957
		RBT	2.1236	1.8025	1.4017	2.4593	1.8645	1.5481	1.1553	2.1962
	3	TBT	1.5249	1.1717	0.8069	1.9619	1.3008	0.9612	0.6136	1.7235
		RBT	1.5340	1.1807	0.8135	1.9696	1.3014	0.9617	0.6141	1.7240
10	1	TBT	3.1732	3.1777	3.1879	3.1700	2.8970	2.8979	2.9015	2.8965
		RBT	3.1795	3.1876	3.2046	3.1736	2.8974	2.8986	2.9026	2.8968
	1.5	TBT	2.5498	2.3126	1.9690	2.7703	2.2930	2.0611	1.7257	2.5088
		RBT	2.5561	2.3214	1.9812	2.7742	2.2934	2.0617	1.7265	2.5090
	2	TBT	2.1029	1.7737	1.3611	2.4460	1.8616	1.5428	1.1450	2.1949
		RBT	2.1082	1.7800	1.3677	2.4499	1.8620	1.5432	1.1454	2.1952
	3	TBT	1.5162	1.1597	0.7906	1.9562	1.2986	0.9576	0.6082	1.7225
		RBT	1.5184	1.1604	0.7876	1.9590	1.2988	0.9577	0.6080	1.7227

6.2 Tapered sandwich beam type (II)

The maximum dimensionless deflections of beam type (II), with various taper ratios, boundary conditions, gradient indexes and slenderness ratios are presented in Tables 8-10. Contrary to the beam type (I), RBT results in higher deflections in beam type (II) compared to TBT. The difference between the deflections obtained via TBT and RBT is more evident in thick beams again.

Table 9 Maximum dimensionless deflections of beam type (II) with CC supports

p	λ	Theory	L/H =5				L/H =20			
			1-1-1	1-2-1	1-8-1	2-1-2	1-1-1	1-2-1	1-8-1	2-1-2
1	1	TBT	0.8975	0.9353	1.0500	0.8753	0.5998	0.6122	0.6682	0.5950
		RBT	0.9400	1.0060	1.1655	0.8979	0.6030	0.6173	0.6763	0.5971
	1.5	TBT	0.7681	0.7467	0.7433	0.7958	0.4795	0.4433	0.4083	0.5181
		RBT	0.8021	0.8030	0.8238	0.8129	0.4821	0.4474	0.4141	0.5210
	2	TBT	0.6676	0.6186	0.5726	0.7250	0.3929	0.3371	0.2766	0.4552
		RBT	0.7028	0.6709	0.6370	0.7420	0.3956	0.3410	0.2816	0.4567
	3	TBT	0.5307	0.4629	0.3953	0.6159	0.2791	0.2152	0.1522	0.3605
		RBT	0.5647	0.5053	0.4354	0.6368	0.2819	0.2187	0.1560	0.3623
2	1	TBT	0.8790	0.8991	0.9513	0.8661	0.5962	0.6014	0.6226	0.5941
		RBT	0.9043	0.9399	1.0198	0.8800	0.5982	0.6045	0.6275	0.5954
	1.5	TBT	0.7403	0.7091	0.6627	0.7848	0.4752	0.4325	0.3765	0.5166
		RBT	0.7626	0.7369	0.7067	0.7908	0.4765	0.4347	0.3799	0.5221
	2	TBT	0.6448	0.5813	0.5047	0.7124	0.3880	0.3268	0.2532	0.4534
		RBT	0.6609	0.6065	0.5380	0.7189	0.3895	0.3289	0.2560	0.4541
	3	TBT	0.5061	0.4275	0.3428	0.6009	0.2738	0.2064	0.1378	0.3580
		RBT	0.5208	0.4465	0.3620	0.6089	0.2752	0.2082	0.1399	0.3589
5	1	TBT	0.8633	0.8710	0.8878	0.8577	0.5939	0.5951	0.5992	0.5933
		RBT	0.8745	0.8888	0.9179	0.8640	0.5950	0.5966	0.6015	0.5941
	1.5	TBT	0.7292	0.6804	0.6099	0.7748	0.4724	0.4263	0.3602	0.5155
		RBT	0.7289	0.6865	0.6234	0.7719	0.4729	0.4270	0.3615	0.5148
	2	TBT	0.6261	0.5531	0.4597	0.7012	0.3850	0.3209	0.2411	0.4521
		RBT	0.6271	0.5577	0.4681	0.6984	0.3854	0.3216	0.2421	0.4522
	3	TBT	0.4864	0.4011	0.3076	0.5880	0.2705	0.2013	0.1302	0.3563
		RBT	0.4861	0.4020	0.3079	0.5855	0.2709	0.2019	0.1309	0.3565
10	1	TBT	0.8570	0.8607	0.8681	0.8541	0.5933	0.5936	0.5947	0.5930
		RBT	0.8626	0.8696	0.8832	0.8573	0.5940	0.5946	0.5960	0.5936
	1.5	TBT	0.7222	0.6699	0.5930	0.7633	0.4717	0.4250	0.3574	0.5152
		RBT	0.7175	0.6677	0.5943	0.7706	0.4717	0.4250	0.3574	0.5152
	2	TBT	0.6188	0.5429	0.4450	0.6966	0.3842	0.3196	0.2389	0.4517
		RBT	0.6140	0.5396	0.4431	0.6900	0.3842	0.3196	0.2389	0.4517
	3	TBT	0.4789	0.3915	0.2957	0.5828	0.2697	0.2002	0.1287	0.3559
		RBT	0.4729	0.3854	0.2884	0.5761	0.2697	0.2002	0.1287	0.3559

Since the facings are homogenous and composed of ceramic, as the face-sheet thickness to core height ratio increases, the stiffness will be increased. This will lead to smaller strains and deflections. Another important finding is that unlike beam type (I), an increment in the gradient index increases the volume fraction of the ceramic constituent. This also results in smaller deflections, bending and shear stresses.

Table 10 Maximum dimensionless deflections of beam type (II) with FC supports

p	λ	Theory	L/H =5				L/H =20			
			1-1-1	1-2-1	1-8-1	2-1-2	1-1-1	1-2-1	1-8-1	2-1-2
1	1	TBT	29.1648	29.7903	32.5501	28.9213	27.9245	28.4441	30.9593	27.7545
		RBT	29.3223	30.0635	33.0070	28.9969	27.9358	28.4629	30.9902	27.7604
	1.5	TBT	20.5413	18.0495	15.3083	23.2247	19.3999	16.8622	14.0224	22.1176
		RBT	20.6239	18.1637	15.4036	23.2651	19.4061	16.8707	14.0302	22.1215
	2	TBT	15.2051	12.0315	8.7559	19.0400	14.1318	10.9529	7.6626	17.9709
		RBT	15.2184	12.0344	8.6913	19.0469	14.1338	10.9545	7.6602	17.9722
	3	TBT	9.2463	6.4050	3.9552	13.4194	8.2933	5.4952	3.1084	12.4264
		RBT	9.1748	6.2939	3.7754	13.3742	8.2902	5.4898	3.0988	12.4246
2	1	TBT	28.9723	29.2392	30.2969	28.8584	27.7938	27.9989	28.9273	27.7251
		RBT	29.0587	29.3894	30.5603	28.8981	27.8004	28.0097	28.9454	27.7287
	1.5	TBT	20.3026	17.5228	14.0158	23.1348	19.2303	16.4442	12.9197	22.0678
		RBT	20.3174	17.5445	14.0240	23.1365	19.2321	16.4466	12.9218	22.0689
	2	TBT	14.9438	11.5616	7.9203	18.9257	13.9458	10.5921	6.9950	17.9028
		RBT	14.8980	11.4987	7.8200	18.8913	13.9439	10.5892	6.9900	17.9013
	3	TBT	8.9845	6.0465	3.5150	13.2713	8.1114	5.2413	2.8043	12.3325
		RBT	8.8707	5.9057	3.3423	13.1865	8.1053	5.2337	2.7948	12.3281
5	1	TBT	28.8438	28.9084	29.1218	28.8098	27.7213	27.7586	27.9193	27.7082
		RBT	28.8723	28.9638	29.2279	28.8180	27.7241	27.7632	27.9272	27.7097
	1.5	TBT	20.1473	17.2092	13.3337	23.0696	19.1370	16.2214	12.3829	22.0403
		RBT	20.1085	17.1595	13.2652	23.0371	19.1353	16.2193	12.3795	22.0366
	2	TBT	14.7774	11.2826	7.4754	18.8454	13.8443	10.4022	6.6734	17.8644
		RBT	14.6842	11.1671	7.3325	18.7762	13.8393	10.3958	6.6650	17.8608
	3	TBT	8.8192	5.8324	3.2715	13.1708	8.0134	5.1100	2.6592	12.2804
		RBT	8.6713	5.6641	3.0897	13.0536	8.0050	5.1004	2.6488	12.2738
10	1	TBT	28.8065	28.8285	28.8871	28.7925	27.7077	27.7156	27.7479	27.7040
		RBT	28.8121	28.8475	28.9315	28.7877	27.7090	27.7178	27.7517	27.7053
	1.5	TBT	20.1053	17.1343	13.1907	23.0480	19.1198	16.1820	12.2913	22.0344
		RBT	20.0446	17.0556	13.0868	23.0011	19.1167	16.1778	12.2859	22.0320
	2	TBT	14.7321	11.2135	7.3746	18.8198	13.8257	10.3684	6.6184	17.8570
		RBT	14.6202	11.0769	7.2115	18.7369	13.8194	10.3600	6.6090	17.8525
	3	TBT	8.7741	5.7767	3.2101	13.1405	7.9955	5.0865	2.6340	12.2705
		RBT	8.6124	5.5963	3.0208	13.0104	7.9861	5.0760	2.6230	12.2631

Table 11 gives the maximum normalized bending stress $\sigma^*_{\max}$ for a simply supported beam of type (II). It must be noted that the facings are homogenous and thus the maximum bending stress occurs at $z = \pm(h(x)+h_f)$ along the beam length. Based on Table 11, the bending stresses obtained via RBT are larger than those obtained by TBT. This takes place because the shear correction factor for rectangular functionally graded cross sections is not equal to $\frac{5}{6}$ and thus this correction factor results in smaller strains compared to RBT theory.

Table 11 Maximum non-dimensional bending stress σ^*_{max} for beam type (II) with SS supports

p	λ	Theory	L/H =5				L/H =20			
			1-1-1	1-2-1	1-8-1	2-1-2	1-1-1	1-2-1	1-8-1	2-1-2
1	1	TBT	3.7785	3.8481	4.1872	3.7561	15.1141	15.3924	16.7489	15.0245
		RBT	3.8476	3.9264	4.2801	3.8182	15.1313	15.4118	16.7720	15.0398
	1.5	TBT	3.2509	3.1054	3.0302	3.4182	13.0038	12.4217	12.1209	13.6731
		RBT	3.3214	3.1884	3.1305	3.4820	13.0217	12.4422	12.1454	13.6890
	2	TBT	2.8546	2.6056	2.3752	3.1371	11.4186	10.4227	9.5011	12.5485
		RBT	2.9312	2.6954	2.4877	3.2033	11.4375	10.4443	9.5268	12.5649
	3	TBT	2.2978	1.9737	1.6590	2.6956	9.1912	7.8949	6.6363	10.7826
		RBT	2.3839	2.0786	1.8055	2.7672	9.2110	7.9187	6.6693	10.8001
2	1	TBT	3.7613	3.7886	3.9134	3.7524	15.0454	15.1545	15.6538	15.0097
		RBT	3.8244	3.8572	3.9916	3.8112	15.0610	15.1715	15.6732	15.0243
	1.5	TBT	3.2288	3.0412	2.8089	3.4127	12.9154	12.1651	11.2357	13.6510
		RBT	3.2939	3.1133	2.8933	3.4724	12.9315	12.1829	11.2563	13.6658
	2	TBT	2.8292	2.5411	2.1909	3.1298	11.3168	10.1647	8.7639	12.5193
		RBT	2.8978	2.6190	2.2859	3.1914	11.3336	10.1833	8.7854	12.5346
	3	TBT	2.2688	1.9131	1.5217	2.6853	9.0753	7.6527	6.0871	10.7415
		RBT	2.3456	2.0043	1.6465	2.7513	9.0928	7.6733	6.1314	10.7575
5	1	TBT	3.7520	3.7568	3.7781	3.7504	15.0080	15.0273	15.1127	15.0017
		RBT	3.8097	3.8170	3.8430	3.8061	15.0223	15.0422	15.1287	15.0155
	1.5	TBT	3.2168	3.0072	2.7009	3.4097	12.8675	12.0291	10.8038	13.6389
		RBT	3.2757	3.0690	2.7707	3.4658	12.8820	12.0446	10.8207	13.6528
	2	TBT	2.8154	2.5072	2.1017	3.1258	11.2618	10.0290	8.4070	12.5034
		RBT	2.8771	2.5747	2.1804	3.1832	11.2769	10.0450	8.4244	12.5176
	3	TBT	2.2533	1.8816	1.4559	2.6797	9.0133	7.5267	5.8236	10.7191
		RBT	2.3218	1.9604	1.5596	2.7408	9.0287	7.5445	5.8638	10.7339
10	1	TBT	3.7503	3.7513	3.7554	3.7500	15.0015	15.0053	15.0219	15.0003
		RBT	3.8058	3.8081	3.8147	3.8044	15.0152	15.0193	15.0365	15.0137
	1.5	TBT	3.2147	3.0014	2.6829	3.4092	12.8591	12.0056	10.7316	13.6368
		RBT	3.2710	3.0600	2.7464	3.4637	12.8730	12.0201	10.7470	13.6504
	2	TBT	2.8130	2.5014	2.0869	3.1251	11.2523	10.0056	8.3476	12.5006
		RBT	2.8718	2.5644	2.1584	3.1808	11.2667	10.0205	8.3632	12.5144
	3	TBT	2.2506	1.8763	1.4449	2.6788	9.0026	7.5052	5.7798	10.7152
		RBT	2.3156	1.9498	1.5394	2.7377	9.0171	7.5216	5.8181	10.7295

Pushover curves of the maximum bending stress are presented in Fig. 5 for a simply supported beam type (II). The effect of gradient indexes and cross sectional types on bending stresses is obvious in these figures. As it can be seen, the gradient indexes are more influential in cross sectional types with large core height to facing thickness ratios, e.g 1-8-1. As p increases from 5 to 10, the pushover curves are marginally affected. According to the this outcome, the effect of gradient index on bending stress can be disregarded for $p \geq 5$. Another important result is that the maximum bending stress will not occur at the mid-span of beams with $\lambda > 1$. In fact, as the taper

ratio and the core height increase, the point at which the maximum bending stress occurs will be shifted leftwards of the mid-span (see Fig. 5(c)). Moreover, for cross sectional types in which the facings are thicker than the core, the effect of gradient index on maximum bending stress is negligible. Fig. 6 is presented to illustrate the pushover curves of the maximum shear stress for a FC beam type (II). It must be reminded that the considered beam is clamped at $x = \xi + L$. As it is expected, the maximum shear stress occurs in the vicinity of the clamped edge. In addition, the difference between the shear stresses related to various gradient indexes becomes more evident as the core height increases. It is important to note that the Ritz method is an assymptotic solution and results in zero shear strains, and shear stresses in the clamped support. Based on the Saint Venant's principle, the distribution of strains and stresses near the supports can be neglected. Hence, the pushover curves are accurate at every point except near the region of clamped edge.

5. Conclusions

In this research, static analysis of tapered FG sandwich beams was carried out. The core height was assumed to vary linearly along the *x* direction. Moreover, two different beam types in which the material properties followed a power-law form were considered. In order to obtain the deflections, the well-known Ritz method was implemented.

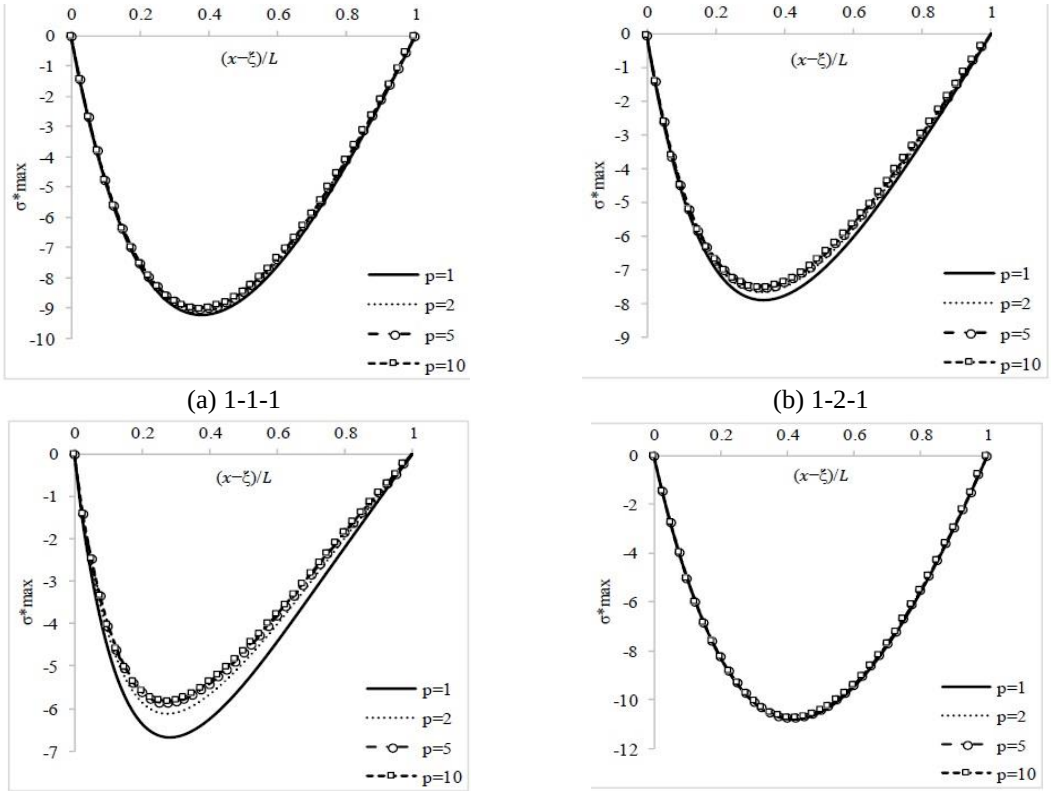

(a) 1-1-1 (b) 1-2-1

(c) 2-1-2 (d) 1-8-1

Fig. 5 The effect of cross sectional type and gradient index on $\sigma^*_{\max}(x,z)$ pushover curves of a simply supported beam type (II), $L/H = 20$, $\lambda = 3$

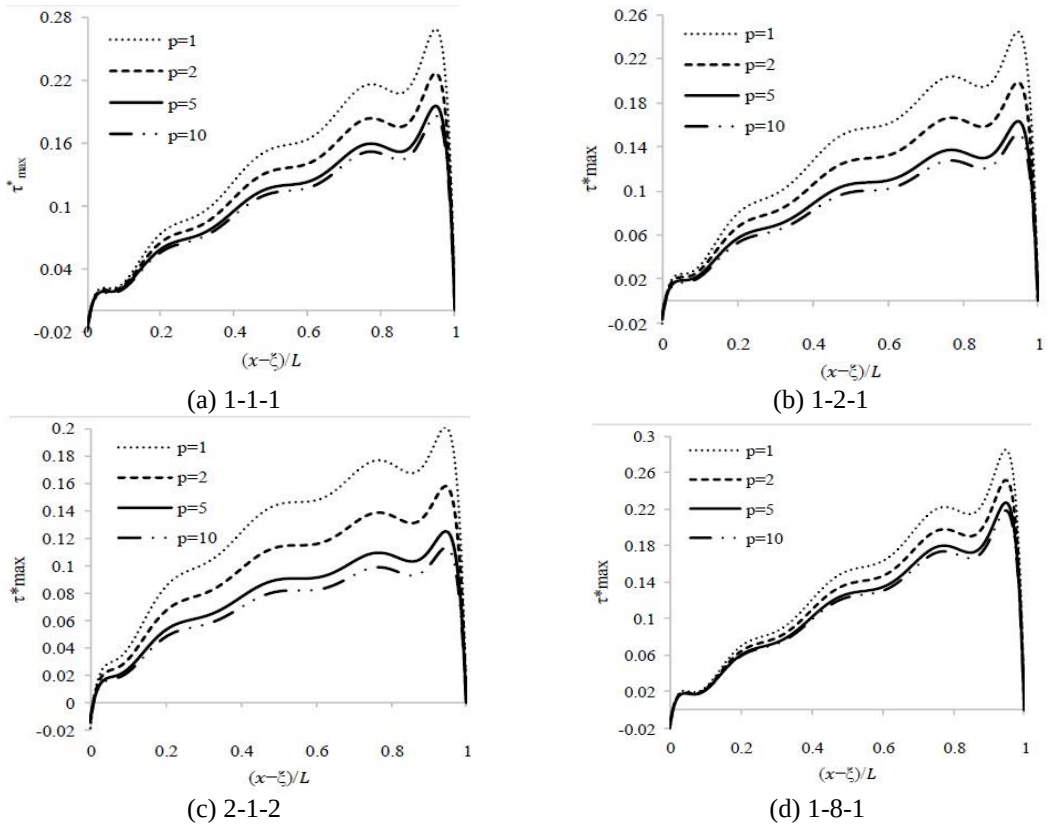

(a) 1-1-1 (b) 1-2-1

(c) 2-1-2 (d) 1-8-1

Fig. 6 The effect of cross sectional type and gradient index on $\tau^*_{\max}(x,z)$ pushover curves of beam type (II) with FC supports, $L/H=20$

Through a convergence study, it was shown that the Chebyshev polynomials offer a remarkable rate of convergence in analysis of FG non-prismatic sections. On the other hand, both Timoshenko and Reddy beam theories were applied, and the results were compared. It was shown that TBT leads to larger deflections, and smaller shear stresses compared to RBT for beam type (I). However, for beam type (II), TBT leads to smaller deflections and bending stresses compared to RBT. It was also observed that the taper ratio, slenderness, cross sectional type and gradient index had significant effects on static responses. The shear effects were found to be more considerable in FG tapered sandwich beams with small slenderness and large taper ratios. Therefore, appropriate responses can be achieved by imposing certain geometrical characteristics and gradient indexes to the beam profile. The outcomes of the present study may provide the researchers with useful results for design of structures, which make use of FG tapered sandwich beams.

References

Ai, Q. and Weaver, P.M. (2017), “Simplified analytical model for tapered sandwich beams using variable

stiffness materials", *J. Sandw. Struct. Mater*., **19**(1), 3-25.
Banić, D., Bacciocchi, M., Tornabene, F. and Ferreira, A. (2017), "Influence of winkler-pasternak foundation on the vibrational behavior of plates and shells reinforced by agglomerated carbon nanotubes", *Appl. Sci*., **7**(12), 1228.
Bourada, M., Kaci, A., Houari, M.S.A. and Tounsi, A. (2015), "A new simple shear and normal deformations theory for functionally graded beams", *Steel Compos. Struct*., **18**(2), 409-423.
Calim, F.F. (2016), "Transient analysis of axially functionally graded Timoshenko beams with variable cross-section", Compos.Part B: Eng., 98(Supplement C), 472-483.
Davoodinik, A.R. and Rahimi, G.H. (2011), "Large deflection of flexible tapered functionally graded beam", *Acta Mechanica Sinica*, **27**(5), 767.
El Meiche, N., Tounsi, A., Ziane, N., Mechab, I. and Adda.Bedia, E.A. (2011), "A new hyperbolic shear deformation theory for buckling and vibration of functionally graded sandwich plate", *Int. J. Mech. Sci*., **53**(4), 237-247.
Fahsi, B., Kaci, A., Tounsi, A. and Bedia, E.A.A. (2012), "A four variable refined plate theory for nonlinear cylindrical bending analysis of functionally graded plates under thermomechanical loadings", *J. Mech. Sci. Technol*., **26**(12), 4073-4079.
Filippi, M., Carrera, E. and Zenkour, A.M. (2015), "Static analyses of FGM beams by various theories and finite elements", *Compos. Part B: Eng*., **72**, 1-9.
Frostig, Y. (2009), "Elastica of sandwich panels with a transversely flexible core-A high order theory approach", *Int. J. Solids Struct*., **46**, 2043-2059.
Frostig, Y., Baruch, M., Vilnay, O. and Sheinman, I. (1992), "Bending of nonsymmetric sandwich beams with flexible core-bending behavior", *J. Eng. Mech*., **117**(9), 1931-1952.
Frostig, Y. and Thomsen, O.T. (2004), "High-order free vibration of sandwich panels with a flexible core", *Int. J. Solids Struct*., **41**, 1697-1724.
Ha, K.H. (1990), "Finite element analysis of sandwich plates: An overview", *Comput. Struct*., **37**(4), 397-403.
Hu, H., Belouettar, S., Potier-Ferry, M. and Daya, M. (2008), "Review and assessment of various theories for modeling sandwich composites", *Compos. Struct*., **84**, 282-292.
Kahya, V. (2016), "Buckling analysis of laminated composite and sandwich beams by the finite element method", *Compos. Part B: Eng*., **91**, 126-134.
Li, S., Hu, J., Zhai, C. and Xie, L. (2013), "A unified method for modeling of axially and/or transversally functionally graded beams with variable cross-section profile", *Mech. Based Des. Struct. Mach*., **41**(2), 168-188.
Liu, H., Liu, H. and Yang, J. (2017), "Clamped sandwich beams with thick weak cores from central impact: A theoretical study", Composite Structures In Press.
Mashat, D.S., Carrera, E., Zenkour, A.M., Al Khateeb, S.A. and Filippi, M. (2014), "Free vibration of FGM layered beams by various theories and finite elements", *Compos. Part B: Eng*., **59**, 269-278.
Masoodi, A.R. and Moghaddam, S.H. (2015), "Nonlinear dynamic analysis and natural frequencies of gabled frame having flexible restraints and connections", *J. Civil Eng. – KSCE*, **19**(6), 1819-1824.
Merdaci, S., Tounsi, A., Houari, M.S.A., Mechab, I., Hebali, H. and Benyoucef, S. (2011), "Two new refined shear displacement models for functionally graded sandwich plates", *Arch. Appl. Mech*., **81**(11), 1507-1522.
Natarajan, S. and Manickam, G. (2012), "Bending and vibration of functionally graded material sandwich plates using an accurate theory", *Finite Elem. Anal. Des*., **57**, 32-42.
Nguyen, D.K. and Gan, B.S. (2014), "Large deflections of tapered functionally graded beams subjected to end forces", *Appl. Math. Model*., **38**(11), 3054-3066.
Nguyen, N.T., Kim, N.I., Cho, I., Phung, Q.T. and Lee, J. (2014), "Static analysis of transversely or axially functionally graded tapered beams", *Mater. Res. Innov*., **18**(2), S2-260-S262-264.
Nguyen, T.K., Nguyen, N.D., Vo, T.P. and Thai, H.T. (2017), "Trigonometric-series solution for analysis of laminated composite beams", *Compos. Struct*., **160**, 142-151.
Nguyen, T.K., Vo, T.P. and Thai, H.T. (2014), "Vibration and buckling analysis of functionally graded

sandwich plates with improved transverse shear stiffness based on the first-order shear deformation theory", *J. Mech. Eng. Sci*., **228**(12), 2110-2131.
Nguyen, V.H., Nguyen, T.K., Thai, H.T. and Vo, T.P. (2014), "A new inverse trigonometric shear deformation theory for isotropic and functionally graded sandwich plates", *Compos. Part B: Eng*., **66**, 233-246.
Niknam, H., Fallah, A. and Aghdam, M.M. (2014), "Nonlinear bending of functionally graded tapered beams subjected to thermal and mechanical loading", *Int. J. Nonlinear Mech.*, **65**(Supplement C), 141-147.
Panteghini, A. and Bardella, L. (2017), "Structural theory and finite element modelling of linear elastic sandwich beams subject to severe boundary conditions", *Eur. J. Mech.- A/Solids*, **61**, 393-407.
Phan, C.N., Kardomateas, G.A. and Frostig, Y. (2013), "Blast response of a sandwich beam/wide plate based on the extended high order sandwich panel theory and comparison with elasticity", *J. Appl. Mech*., **80**(6), 1-11.
Pradhan, K.K. and Chakraverty, S. (2013), "Free vibration of Euler and Timoshenko functionally graded beams by Rayleigh–Ritz method", *Compos. Part B: Eng*., **51**(Supplement C), 175-184.
Rajasekaran, S. (2013), "Free vibration of centrifugally stiffened axially functionally graded tapered Timoshenko beams using differential transformation and quadrature methods", *Appl. Math. Model*., **37**(6), 4440-4463.
Rezaiee-Pajand, M. and Hozhabrossadati, S.M. (2016), "Analytical and numerical method for free vibration of double-axially functionally graded beams", *Compos. Struct*., **152**, 488-498.
Rezaiee-Pajand, M. and Masoodi, A.R. (2016), "Exact natural frequencies and buckling load of functionally graded material tapered beam-columns considering semi-rigid connections", J. Vib. Control In Press.
Rezaiee-Pajand, M., Sani, A.A. and Hozhabrossadati, S.M. (2017), "Application of differential transform method to free vibration of gabled frames with rotational springs", *Int. J. Struct. Stab. Dynam.*, **17**(1), 1750012.
Santiuste, C., Thomsen, O.T. and Frostig, Y. (2011), "Thermo-mechanical load interactions in foam cored axi-symmetric sandwich circular plates-High-order and FE models", *Compos. Struct*., **93**, 369-376.
Shafiei, N. and Kazemi, M. (2017), "Buckling analysis on the bi-dimensional functionally graded porous tapered nano-/micro-scale beams", *Aerosp. Sci. Technol*., **66**(Supplement C), 1-11.
Shafiei, N., Mousavi, A. and Ghadiri, M. (2016), "Vibration behavior of a rotating non-uniform FG microbeam based on the modified couple stress theory and GDQEM", *Compos. Struct*., **149**(Supplement C), 157-169.
Simsek, M. (2010), "Fundamental frequency analysis of functionally graded beams by using different higher-order beam theories", *Nuclear Eng. Des*., **240**, 697-705.
Sobhy, M. (2013), "Buckling and free vibration of exponentially graded sandwich plates resting on elastic foundations under various boundary conditions", *Compos. Struct*., **99**, 76-87.
Thai, C.H., Kulasegaram, S., Tran, L.V. and Nguyen-Xuan, H. (2014), "Generalized shear deformation theory for functionally graded isotropic and sandwich plates based on isogeometric approach", *Comput. Struct*., **141**, 94-112.
Thai, H.T., Nguyen, T.K., Vo, T.P. and Lee, J. (2014), "Analysis of functionally graded sandwich plates using a new first-order shear deformation theory", *Eur. J. Mech.- A/Solids*, **45**, 211-225.
Thai, H.T., Vo, T.P., Nguyen, T.K. and Lee, J. (2015), "Size-dependent behavior of functionally graded sandwich microbeams based on the modified couple stress theory", *Compos. Struct.*, **123**(Supplement C): 337-349.
Tornabene, F., Fantuzzi, N. and Bacciocchi, M. (2017), "Linear static response of nanocomposite plates and shells reinforced by agglomerated carbon nanotubes", *Compos. Part B: Eng*., **115**, 449-476.
Tornabene, F., Fantuzzi, N. and Bacciocchi, M., Viola, E. and Reddy, J. (2017), "A numerical investigation on the natural frequencies of FGM sandwich shells with variable thickness by the local generalized differential quadrature method", *Appl. Sci*., **7**(2), 131.
Venkataraman, S. and Sankar, B.V. (2003), "Elasticity Solution for Stresses in a Sandwich Beam with Functionally Graded Core", *AIAA J*., **41**(12), 2501-2505.

Vinson, J.R. (1999), The Behavior of Sandwich Structures of Isotropic and Composite Materials. New York, CRC Press

Vo, T.P., Thai, H.T., Nguyen, T.K., Inam, F. and Lee, J. (2015), "A quasi-3D theory for vibration and buckling of functionally graded sandwich beams", *Compos. Struct*., **119**, 1-12.

Vo, T.P., Thai, H.T., Nguyen, T.K., Inam, F. and Lee, J. (2015), "Static behaviour of functionally graded sandwich beams using a quasi-3D theory", Compos. Part B: Eng., **68**, 59-74.

Xiang, X.M., Lu, G., Ma, G.W., Li, X.Y. and Shu, D.W. (2016), "Blast response of sandwich beams with thin-walled tubes as core", *Eng. Struct*., **127**, 40-48.

Zare Jouneghani, F., Dimitri, R., Bacciocchi, M. and Tornabene, F. (2017), "Free vibration analysis of functionally graded porous doubly-curved shells based on the first-order shear deformation theory", *Appl. Sci*., **7**(12), 1252.

Zenkour, A.M. (2005), "A comprehensive analysis of functionally graded sandwich plates: Part 1—Deflection and stresses", *Int. J. Solids Struct*., **42**(18-19), 5224-5242.

Zenkour, A.M. (2005), "A comprehensive analysis of functionally graded sandwich plates: Part 2—Buckling and free vibration", *Int. J. Solids Struct*., **42**(18-19), 5243-5258.

CC